Crystallite Size and Shape in Twaron Fibers Heat Treated at Different Temperatures Using WAXS

Anjana Jain,[1] S. Abhishek,[2] Sangappa,[3] S. S. Mahesh,[2] R. Somashekar[2]

[1]*Material Science Division, National Aerospace Laboratories, Bangalore 560017, India*
[2]*Department of Studies in Physics, University of Mysore, Manasagangotri, Mysore 570006, India*
[3]*Department of Physics, University of Mangalore, Mangalore 574199, India*

Received 1 September 2004; accepted 7 August 2005
DOI 10.1002/app.23557
Published online in Wiley InterScience (www.interscience.wiley.com).

ABSTRACT: We have determined the crystallite size of Twaron fibers heat treated at various temperatures by analyzing the wide angle X-ray scattering (WAXS) data employing a profile analysis technique developed by us. This study indicates that the differential change of size with temperature is less than 1% of the mean value along both (110) and (200) directions. Hence, these fibers are thermally stable and thermal aging is negligible. We have also observed that the lattice strain variation with temperature is negligible. These studies demonstrate the thermal stability of fibers in terms of the changes in the microcrystalline parameters. © 2006 Wiley Periodicals, Inc. J Appl Polym Sci 100: 4910–4916, 2006

Key words: WAXS; crystal imperfection parameters; crystallite shape; lognormal

INTRODUCTION

Twaron fibers are essentially made up of poly(*p*-phenylene tetrephthalamide) (PPTA), the structural formula being $[—NH—C_6H_4—NH—CO—C_6H_4—CO]_n$. These light weight aramid fibers are of high strength and high modulus, with good thermal stability and high impact resistance, and are extensively used in ballistic applications.[1] Kevlar fibers also are made up of PPTA and are commercialized by DuPont (USA). Extensive studies on thermal exposure of Kevlar fibers have been made by earlier investigators.[2–7] Since Twaron fibers are used in aerospace industry, it is of interest to know the behavior of microcrystalline parameters of these fibers with temperature and hence thermal aging. We have recorded the necessary X-ray data of these fibers at different temperature settings and used the Fourier method of profile analysis developed by us to compute the microcrystalline parameters.[8] The accuracy of the Fourier method has been pointed out in a recently concluded IUCr Round Robin test.[9] Because of their extensive industrial applications, an interpretation of thermal stability of Twaron fibers, in terms of its microcrystalline parameters like crystallite size and strain will be of immense help in understanding the relation between the physical properties like tensile strength and molecular ordering (characterized by shape and size of the crystallites) in these fibers.

Correspondence to: R. Somashekar (rs@uomphysics.net).

Journal of Applied Polymer Science, Vol. 100, 4910–4916 (2006)

THEORY

Microstructure encompasses the compositional inhomogeneity, the amount and the distribution of the phase in the material, the grain size and shape, the distribution functions of the grain-size parameters, the grain (crystal)-orientation distribution function(texture), the grain boundaries/interfaces, the surface of the material, the concentrations and distributions of crystal defects such as vacancies, dislocations, stacking and twin faults, and not being in the last place, lattice distortions due to strains/stresses, etc.[10]

Microstructural parameters like crystal size $\langle N \rangle$ and lattice strain (g in %) are usually determined by employing the Fourier method of Warren and Averbach.[11–13] The intensity of a profile, in the direction joining the origin to the center of the reflection, can be expanded in terms of a Fourier cosine series:

$$I(s) = \sum_{n=-\infty}^{\infty} A(n) \cos\{2\pi n d(s - s_o)\} \qquad (1)$$

where the coefficients of the harmonics $A(n)$ are functions of the size of the crystallite and the disorder of the lattice. Here, s is sin $(\theta)/(\lambda)$, s_0 is the value of s at peak of a profile, n is the harmonic order of coefficient, and d is the lattice spacing. The Fourier coefficients can be expressed as

$$A(n) = A_s(n)\, A_d(n) \tag{2}$$

For a paracrystalline material like Twaron fiber, $A_d(n)$ turns out to be a Gaussian strain distribution[13,14]:

$$A_d(n) = \exp\,(-2\pi^2 m^2 n g^2) \tag{3}$$

Here m is the order of the reflection and $g = (\Delta d/d)$ is the lattice strain. Normally, mean square strain $\langle \varepsilon^2 \rangle$ is given by g^2/n. This mean square strain is dependent on n, whereas not on g.[15,16] For a probability distribution of column lengths $P(i)$, we have

$$A_s(n) = 1 - \frac{nd}{D} - \frac{d}{D}\left[\int_0^n iP(n)\, di - n\int_0^n P(i)\, di\right] \tag{4}$$

where $D = \langle N \rangle d_{hkl}$ is the crystallite size and i is the number of unit cells in a column. In the presence of two orders of reflections from the same set of Bragg planes, Warren and Averbach[11] have shown a method of obtaining the crystal size ($\langle N \rangle$) and lattice strain (g in %). But, in Twaron fibers, it is very rare to find multiple reflections. So, to find the finer details of microstructure, we approximate the size profiles by a simple analytical function for $P(i)$. Here, we have considered only asymmetric functions. Another advantage of this method is that the distribution function is different along different directions. Whereas, Ribarik et al., Pope and Balzar, and Scardi and Leoni[17–19] used a single crystal size distribution function for the whole pattern fitting, which, we feel, may be inadequate to describe Twaron fiber diffraction patterns. Here, we would like to emphasize that the Fourier method of profile analysis (single order method used here) is a quite reliable one as per the recent survey and the results of the Round Robin test conducted by IUCr.[9] In fact, for refinement, we have also considered the effect of background by introducing a parameter (see ref. 20 for details regarding the effect of background on the microcrystalline parameters).

The exponential distribution

It is assumed that there are no columns containing fewer than p unit cells and those with more decay exponentially. Thus, we have[8]

$$P(i) = \begin{cases} 0 & \text{if } p < i \\ \alpha \exp\{-\alpha(i-p)\} & \text{if } p \geq i \end{cases} \tag{5}$$

where $\alpha = 1/(N - p)$. Substituting this in eq. (4), we get

$$A_s(n) = \begin{cases} A(0)(1 - n/\langle N \rangle) & \text{if } n \leq p \\ A(0)\{\exp[-\alpha(n-p)]\}/(\alpha N) & \text{if } n \geq p \end{cases} \tag{6}$$

Here α is the width of the distribution function, i is the number of unit cells in a column, n is the harmonic number, p is the smallest number of unit cells in a column, and N is the number of unit cells counted in a direction perpendicular to the (hkl) Bragg plane.

The lognormal distribution

The lognormal distribution function is given by

$$P(i) = \frac{1}{(2\pi)^{1/2}\sigma}\frac{1}{i}\exp\left\{-\frac{[\log(i/m)]^2}{2\sigma^2}\right\} \tag{7}$$

where σ is the variance and m is the median of the distribution function.

Substituting eq. (7) in eq. (4) and simplifying,[17] we get

$$\begin{aligned} A_s(n) = {} & \frac{m^3 \exp[(9/4)(2^{1/2}\sigma)^2}{3}\operatorname{erfc}\left[\frac{\log(|n|/m)}{2^{1/2}\sigma} - \frac{3}{2}2^{1/2}\sigma\right] \\ & - \frac{m^2 \exp(2^{1/2}\sigma)^2}{2}|n|\operatorname{erfc}\left[\frac{\log(|n|/m)}{2^{1/2}\sigma} - 2^{1/2}\sigma\right] \\ & + \frac{|n|^3}{6}\operatorname{erfc}\left[\frac{\log(|n|/m)}{2^{1/2}\sigma}\right] \end{aligned} \tag{8}$$

The previous equation is the one used in ref. 17. The maximal value $A_s(0)$ is given by

$$A_s(0) = \frac{2m^3 \exp[(9/4)(2^{1/2}\sigma)^2]}{3} \tag{9}$$

The area-weighted number of unit cell in a column is given by

$$\langle N \rangle_{\text{surf}} = \frac{2m \exp[(5/4)(2^{1/2}\sigma)^2]}{3} \tag{10}$$

and the volume-weighted number of the unit cell in a column is given by

$$\langle N \rangle_{\text{vol}} = \frac{3m \exp[(7/4)(2^{1/2}\sigma)^2}{4} \tag{11}$$

All the distribution functions were put to test to find out the most suitable crystal size distribution function for the profile analysis of the X-ray fiber diffraction. The procedure adopted for the computation of the parameters was as follows. Initial values of g and N were obtained using the method of Nandi et al.[16] With these values in the equations mentioned earlier, one gets the corresponding values for the width of distribution. These are only rough estimates, and therefore the refinement procedure must be sufficiently robust to start with such values. Here, we compute

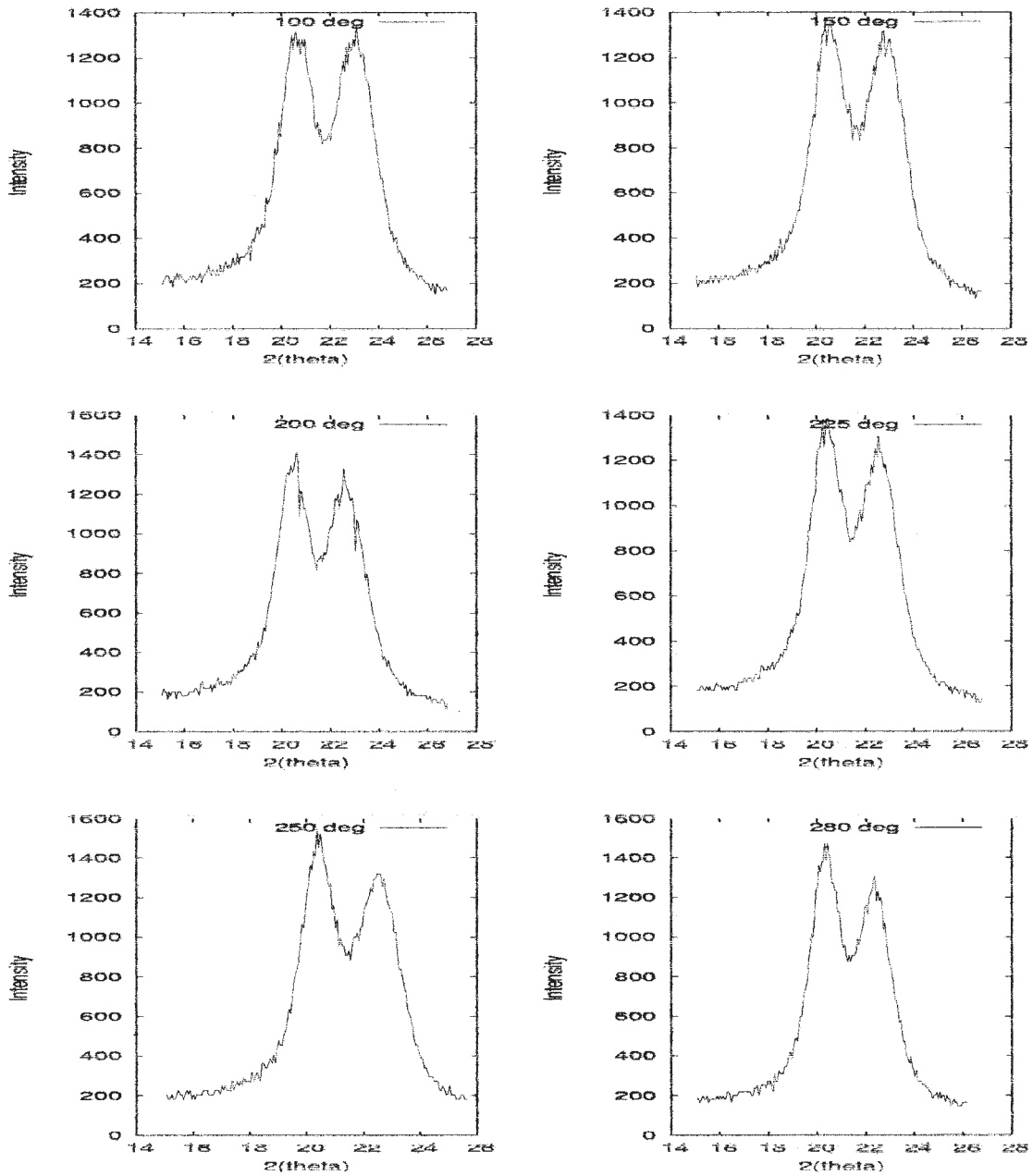

Figure 1 X-ray recordings of Twaron fibers at different temperatures [(200) and (110) reflections].

$$\Delta^2 = [I_{cal} - (I_{exp} + BG)]^2/npt \qquad (12)$$

where BG parameter represents the error in the background estimation, *npt* is number of data points in a profile, I_{cal} is intensity calculated using eq. (1), and I_{exp} is the experimental intensity. The values of Δ were divided by half the maximum value of intensity to be expressed relative to the mean value of intensities, and then minimized. For refinement against intensities, the multidimensional minimization algorithm of the SIMPLEX method was used.[21]

EXPERIMENTAL

The Twaron fibers used in the present study were provided by the kind courtesy of Akzo Nobel, the Netherlands. The temperatures chosen for our study were 30, 50, 100, 150, 200, 225, 250, and 280°C. The duration of the cumulative exposures, t_{cum}, varied with the value of T. The decomposition temperature, T_d, reported[22] for Twaron is 500°C. Unconstrained bundles of fibers, ~50 mm in length and ~2 mm thick, were aged in air, using a tubular resistance furnace with nichrome as the heating element. By employing a proportional, integral, and differential (PID) controller, the temperature of the furnace

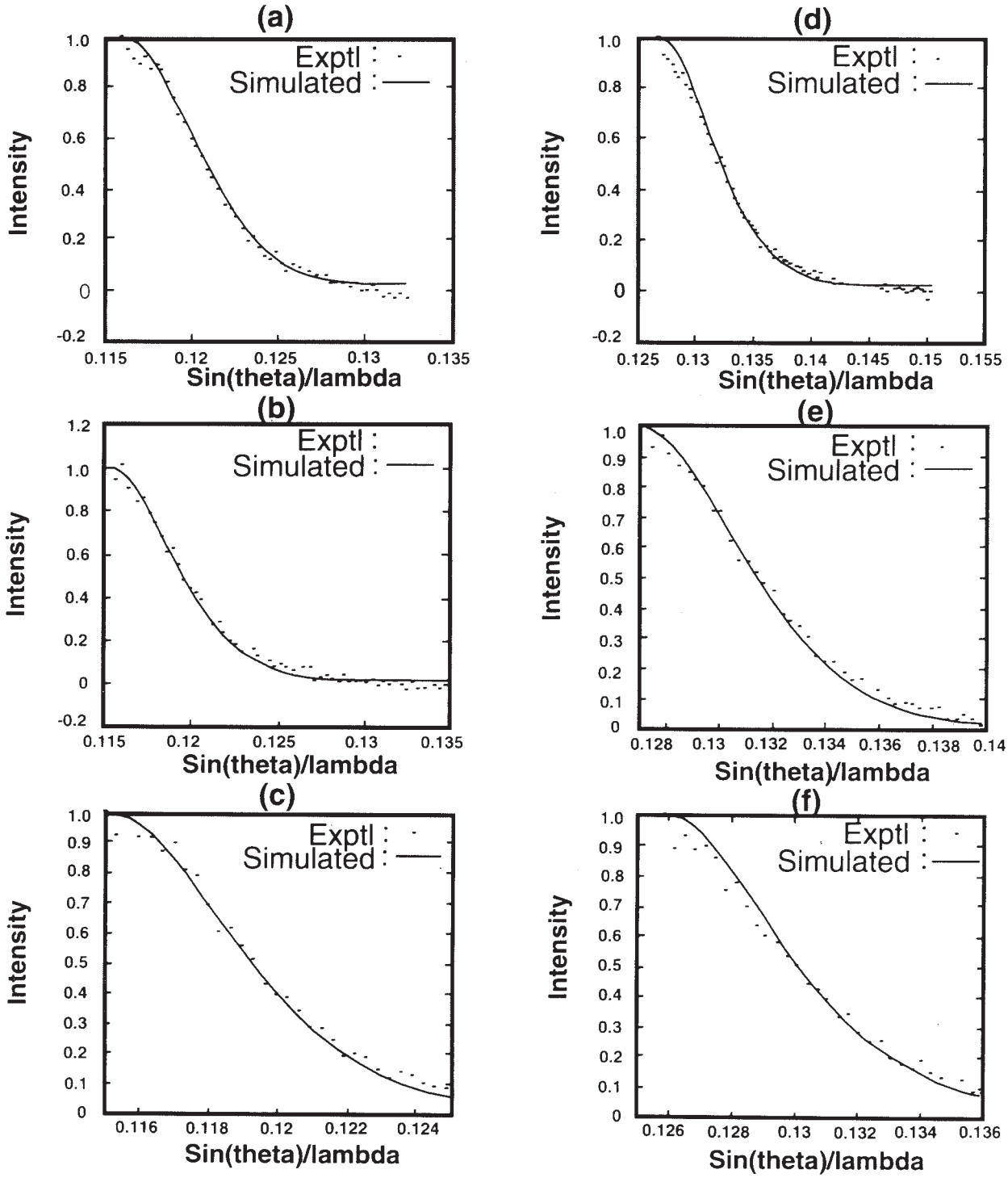

Figure 2 Simulated and experimental profiles of Twaron fibers at different temperatures. (a), (b), (c) (110) reflection; (d), (e), (f) (200) reflection.

could be controlled to an accuracy of ±1°C. The temperature of the sample was measured using a chromel–alumel thermocouple. Fibers encased in a quartz tube were slid into the constant temperature zone (CTZ) of the furnace, prestabilized at a chosen temperature. At various stages of aging, the samples were taken out, air cooled, and characterized. The technique used for the characterization of fibers, prior to and at various stages of heat treatment, was X-ray diffraction. It must be mentioned that separate bundles of fibers were used for the various types of analyses. At every stage of the analysis, extreme care was exercised to ensure that the samples were not contaminated by dust or dirt and were not subjected to any other type of mishandling.

TABLE I
Microstructural Parameters of Twaron Fibers Along (110) Direction

	Exponential					Lognormal					
Temperature (°C)	$\langle N\rangle_{surf}$	g (%)	BG	α	Δ	$\langle N\rangle$surf	g (%)	BG	$\langle N\rangle_{vol}$	Δ	Tensile strength ratio $S(T)/S(o)$
30	11.0 ± 0.8	0.1	−0.2	0.3 ± 0.02	0.07	10.6 ± 0.8	0.1	−0.06	11.9 ± 0.9	0.07	0.98
50	9.3 ± 0.7	0.1	−2.0	0.4 ± 0.03	0.07	8.8 ± 0.6	0.1	−0.07	9.9 ± 0.7	0.07	1.00
100	10.5 ± 0.8	0.1	−1.5	0.3 ± 0.02	0.08	10.2 ± 0.9	0.1	−0.06	11.4 ± 1.1	0.09	1.05
150	9.2 ± 0.6	0.1	−0.2	0.2 ± 0.01	0.06	9.6 ± 0.9	0.3	−0.07	10.8 ± 1.0	0.09	1.02
200	9.4 ± 0.5	0.1	−0.13	0.4 ± 0.02	0.05	9.4 ± 0.6	3.0	−0.13	10.6 ± 0.6	0.06	0.93
225	10.0 ± 0.5	0.1	−0.1	0.2 ± 0.01	0.05	10.8 ± 0.8	2.5	−0.07	12.2 ± 0.9	0.07	1.01
250	10.3 ± 0.6	0.1	−1.3	0.3 ± 0.02	0.06	10.6 ± 0.7	3.0	−0.08	12.0 ± 0.8	0.07	0.73
280	10.2 ± 0.6	0.1	−1.3	0.3 ± 0.02	0.06	9.6 ± 0.7	0.1	−0.07	10.9 ± 0.8	0.07	0.58

Wide-angle X-ray diffraction patterns were recorded in the reflection geometry, using a Philips powder diffractometer with a proportional counter and a graphite monochromator in the diffracted beam. Cu Kα radiation was used. The samples were rotated at the rate of 1/4° per minute, and a chart speed of 10 mm/min was used. It must be emphasized that the geometry of the Philips diffractometer permitted the recording of only the equatorial patterns. Representative X-ray recordings of raw Twaron fiber at different temperatures are shown in Figure 1.

The instrumental broadening corrections were carried out using Stokes method.[23] Standard X-ray profiles, at appropriate 2θ angles of the sample, were obtained from standard samples like ball milled Iron powder and were used for subracting the instrumental broadening by the Stokes deconvolution method. These corrections, even though they are relatively small (less than 5%) in polymeric samples compared with metal oxide compounds, were carried out before the profile analysis. The tensile testing was conducted on a single fiber, using a Zwick universal testing machine. Separate bundles of Twaron fibers were exposed progressively to 30, 50, 100,150, 200, 225, 250, and 280°C. At each of the chosen temperatures, the residence time was 1 h, after which the tensile properties were analyzed. For example, after exposure to 150°C for 1 h, few fibers from the bundle were removed for tensile testing, and the rest of bundle was used for further heating. Prior to the tensile testing, the diameter of each fiber was measured at five different points along the length, and the average value was estimated. A gauge length of 25 mm was selected. The fibers were pulled at a rate of 2.5 mm/min, and a chart speed of 60 mm/min was used to record the load–extension curves. Loads in the range 0–0.5 N were applied to the fibers, using an appropriate load cell. From the load–extension curves, values of tenacity were obtained. Tensile testing could not be carried out for samples exposed to temperatures greater than 350°C, because, at these temperatures, the fibers became too brittle for handling.

RESULTS AND DISCUSSION

Equatorial scanning of the X-ray reflection profile, obtained from Twaron fibers, was used for the estimation of microcrystalline parameters like crystal size (N) and lattice distortion (g in %). In all these computations, we observed that an exponential distribution gave a reasonably good fit, better than the lognormal distribution. Hence, we present the results obtained using an exponential distribution function for crystallite size. Figure 2 shows the experimental and simu-

TABLE II
Microstructural Parameters of Twaron Fibers Along (200) Direction

	Exponential					Lognormal					
Temperature (°C)	$\langle N\rangle_{surf}$	g (%)	BG	α	Δ	$\langle N\rangle_{surf}$	g (%)	BG	$\langle N\rangle_{vol}$	Δ	Tensile strength ratio $S(T)/S(o)$
30	6.0 ± 0.2	0.1	−1.2	0.3 ± 0.01	0.04	7.1 ± 0.4	2.0	−0.01	8.0 ± 0.5	0.06	0.98
50	9.1 ± 0.5	0.1	−1.9	0.4 ± 0.02	0.06	8.6 ± 0.5	0.5	−0.11	9.7 ± 0.6	0.06	1.00
100	9.7 ± 0.5	0.1	−0.2	0.3 ± 0.02	0.05	9.3 ± 0.6	0.5	−0.09	10.5 ± 0.6	0.06	1.05
150	9.1 ± 0.6	0.1	−0.7	0.5 ± 0.03	0.07	9.0 ± 0.6	3.0	−0.08	10.1 ± 0.7	0.07	1.02
200	8.8 ± 0.4	0.1	−0.2	0.4 ± 0.02	0.05	8.4 ± 0.5	0.3	−0.07	9.4 ± 0.6	0.06	0.93
225	9.1 ± 0.5	0.1	−0.3	0.3 ± 0.02	0.05	9.9 ± 0.6	0.1	−0.06	9.9 ± 0.6	0.05	1.01
250	10.6 ± 0.6	0.1	−0.04	0.3 ± 0.002	0.06	10.0 ± 0.7	1.0	−0.11	11.2 ± 0.8	0.07	0.73
280	10.4 ± 0.6	0.1	−1.4	0.3 ± 0.02	0.06	10.8 ± 0.8	3.0	−0.07	12.2 ± 0.9	0.07	0.58

lated intensity profiles for Twaron fibers using the exponential size distribution function. In all the cases, the goodness of the fit, as defined in eq. (12), was less than 15%. Figure 2 shows the comparison between simulated and experimental profiles for raw Twaron fibers for Bragg (110) reflection. The simulated profile was obtained with the aforementioned equations along with the appropriate model parameters. These calculations were carried out for all the other samples treated at different temperatures. The computed microcrystalline parameters like crystalline size (number of unit cells) $\langle N \rangle$, lattice strain (g in %), the width of the crystalline size distribution α, and the goodness of the fit are given in Table I. We have also reproduced the ratio $S(T)/S(O)$, with $S(T)$ as the tenacity at temperature T and $S(O)$ as the tenacity at room temperature.[24] The goodness of fit while computing these tenacity parameters is less than 5%, for all the temperatures. We observe that the lattice strain and its variation for various values of the temperature T in Twaron fibers is very small and is almost insignificant. This is an inherent problem in the model, associated with the present assumption of a functional form for crystallite size distribution. If one considers the variation of crystallite size with temperature, we observe that it is linear, and the extent of linearity is measured by the correlation index which turns to be index, of one; the differential change in crystallite size with temperature, in both directions (110) and (200) is 1% of the mean crystallite value, and this result reflects the thermal stability of the Twaron fibers for a temperature range studied here, and viewed in terms of the microcrystalline parameters (Table II). This result is also supported by the fact that the values of tenacity ratio change corresponding to the temperature. Figure 3 shows the crystallite shape in Twaron fibers at different temperatures; small changes in the shapes occur only at the periphery of these crystallites, which brings out the essence of our results. This implies that these small changes in crystallites of Twaron fibers is due to the breaking of inter- and intra- weak hydrogen bonds like C—H. . . O; N—H. . . O, and O—H. . . O. Scanning electron microscope studies of thermally treated Twaron fibers reported earlier do support the results observed here.[24] In fact, it is observed that there are very few regions on the surface of the fiber with localized pits, sponge-like and wool-like appearances when exposed to different temperatures, which are indicative of small surface changes, and the presence of these regions slightly alters the size of crystallite regions. We also observe a sharp drop in the tenacity at 250°C, and this is not reflected in our X-ray diffraction studies. We do not know the reason for this.

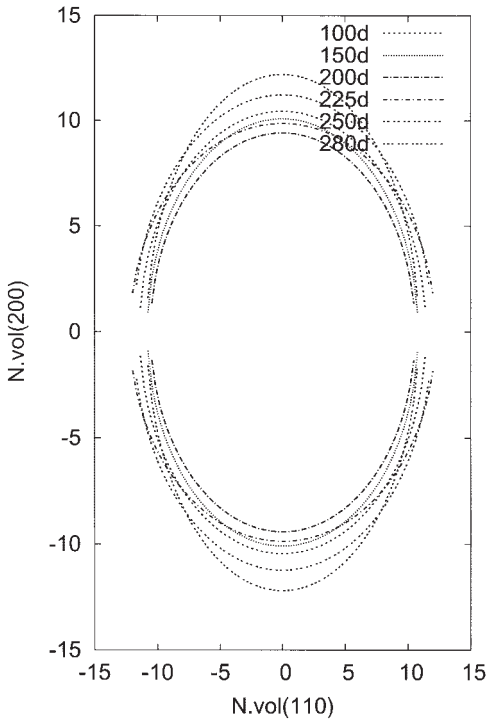

Figure 3 Crystallite shape ellipsoid at different temperatures in Twaron fibers.

CONCLUSIONS

The thermal stability of Twaron fibers has been observed by studying the temperature dependence of crystallite size and shape obtained from X-ray profile analysis, for the first time. The differential change in the size with temperature, within reasonable chosen error margins, mean crystallite size values are constant indicating the thermal stability of molecular configuration in Twaron fibers. This result is also supported by electron microscope studies and tenacity measurements. We have also estimated the lattice residual strain present in these Twaron fibers, and we find that there is negligible change in the strain parameter with temperature within the purview of assumed model functions. All these microstructural results emphasize the thermal stability of twaron fibers for a temperature of 30°C to 280°C.

The authors thank Akzo Nobel for kindly providing Twaron fibers to Ms. Anjana for this study.

References

1. Schuster, D. Twaron in Composites and Protective Clothing; Technical Research Centre of Finland: VTT, Finland, 1992; p 233.
2. Fitzer, E.; Kompalik, D.; Kunz, M. Deutsche Keramischen Gesellschaft EV, 1986; p 847.
3. Hindeleh, A. M.; Abodo, Sh. M. Polymer 1989, 30, 18.
4. Hindeleh, A. M.; Abu Obaid, A. A. Acta Polym 1996, 47, 55.
5. Shubha, M. M.Phil Thesis, Mangalore University, India, 1989.

6. Parimala, H. V.; Vijayan, K. J Mater Sci Lett 1993, 12, 99.
7. Parimala, H. V. M.Phil Thesis, Mangalore University, India, 1991.
8. Somashekar, R.; Somashekarappa, H. J Appl Crystallogr 1997, 30,147.
9. Balzar, D. IUCr Newslett 2002, 28, 14.
10. Mittemeijer, E. J.; Scardi, P., Eds. Diffraction Analysis of the Microstructure of Materials; Springer: Berlin, 2004.
11. Warren, B. E.; Averbach, B. L. J Appl Phys 1950, 21, 595.
12. Warren, B. E. Acta Crystallogr 1955, 8, 483.
13. Warren, B. E. X-ray Diffraction; Addision-Wesley: New York, 1969.
14. Hall, I. H.; Somashekar, R. J Appl Crystallogr 1991, 24, 1051.
15. Rothman, R. L.; Cohen, J. B. J Appl Phys 1971, 24, 971.
16. Nandi, R. K.; Kho, H. K.; Schlosberg, W.; Wissler, G.; Cohen, J. B.; Crist, B., Jr. J Appl Crystallogr 1984, 17, 22.
17. Ribarik, R.; Ungar, T.; Gubicza, J. J Appl Crystallogr 2001, 34, 669.
18. Pope, N. C.; Balzar, D. J Appl Crystallogr 2002, 35, 338.
19. Scardi, P.; Leoni, M. Acta Crystallogr Sect A 2001, 57, 604.
20. Somashekar, R.; Hall, I. H.; Carr, P. D. J Appl Crystallogr 1989, 22, 363.
21. Press, W.; Flannery, B. P.; Teukolsky, S.; Vetterling, W. T., Eds. Numerical Recipes; Cambridge University Press: New York, 1986.
22. Linda, L. C. In Handbook of Composites; Peters, S. T., Ed.; Chapman and Hall: London, 1998; p 206.
23. Stokes, A. R. Proc Phys Soc London 1948, 61, 382.
24. Anjana Jain, Kalyani Vijayan. High Perform Polym 2003, 15, 105.